High Li^+ transference number electrolyte enabled by fluoride-acceptor for low temperature Li-ion batteries

Md Anwar Hossain[1], Dezhen Wu[1], Qijia Zhu[1], Qian Liu[1], Jingtian Yang[1], Jiayi Xu[1], Cong Liu[1], Seungyeop Kang[3], Zhenzhen Yang[1], Seoung-Bum Son[1], Dong-Joo Yoo[3]* and Zhengcheng Zhang[1,2]*

[1]Chemical Sciences and Engineering Division, Argonne National Laboratory, 9700 S. Cass Ave., Lemont, IL 60439, USA

[2]Pritzker School of Molecular Engineering, The University of Chicago, 5640 S. Ellis Ave., Chicago, IL 60637, USA

[3]School of Mechanical Engineering, Korea University, 145 Anam-ro, Seongbuk-gu, Seoul 02841, Republic of Korea

*Corresponding author. E-mail: djyoo@korea.ac.kr; zzhang@anl.gov

TOC

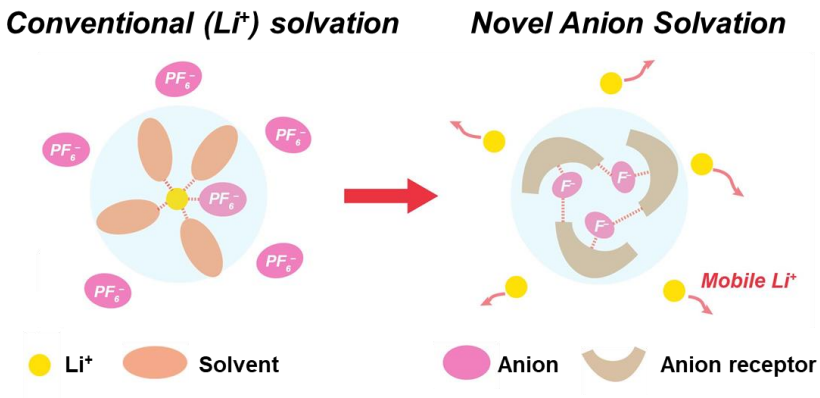
Conventional (Li+) solvation
Novel Anion Solvation
PF6-
F-
Mobile Li+
Li+
Solvent
Anion
Anion receptor

Abstract

To enable wide-temperature operation of lithium-ion batteries (LIBs), new electrolyte formulations have been developed to enhance performance, particularly at low temperatures. A key challenge lies in achieving both high ionic conductivity and a high lithium-ion transference number due to their inherent trade-off. In this study, we designed an electrolyte system comprising tris(pentafluorophenyl) borane (TPFPB), a fluoride acceptor, and LiF salt in ethylene carbonate (EC)-free solvents. TPFPB, with its electron-deficient boron center, facilitates fluoride transfer reactions that promote the dissociation of otherwise insoluble LiF. When methyl acetate (MA) was used as the solvent, the electrolyte exhibited a high transference number ($t_{Li^+} = 0.848$) and ionic conductivity ($\sigma = 5.0 \times 10^{-3}$ S cm^{-1}). The optimized electrolyte demonstrated excellent performance at −20 °C, with no evidence of lithium plating. This work presents a new strategy for electrolyte design by leveraging cation desolvation to achieve high-performance LIBs for low-temperature and high-power applications.

Since the advent of Li-ion batteries (LIBs) in the market, they have been extensively utilized as a power sources for consumer electronics, electric vehicles (EVs) and large-scale stationary energy storage systems due to their balanced performance such as energy density, power capability, cycle/calendar life, and a moderate operating temperature range.[1-3] Although there has been tremendous improvement in the development of active electrode materials to increase the energy density for EV application, the poor performance at low temperatures retards the EV market growth and limits the application in harsh conditions for the use in polar areas or space exploration.[4-6] The battery performance relies on how fast Li ions diffuse in the electrolyte and transfer to electrode materials. All the movements of Li ions within LIBs including graphite anodes, layered oxide cathodes and electrolytes become sluggish at reduced temperatures, especially in the electrolyte. Conventional electrolyte contains low melting point (36.4ºC) ethylene carbonate (EC) solvent, which causes an abrupt decrease in ionic conductivity of electrolytes and large cell overpotential at low temperatures.[7, 8]

EC solvent is also known to dissociate the Li salt to high concentrations and capable of forming a stable solid-electrolyte-interphase (SEI) by multi-electron ring-opening reduction reaction with Li ions. In commercial electrolytes, Li ions are tightly bound by EC solvent forming a typical solvation structure of 1 Li^+:4 EC molecules, and have high solvation/desolvation energies at the electrode interface, inducing high charge-transfer resistances at low temperatures.[6, 9] In addition, the ionic conductivity of carbonate electrolytes has high activation energies, resulting in sluggish ionic conduction at low temperatures. To enhance the ionic conductivity at low temperatures, there have been studies for developing effective electrolyte solvents with various functional groups such as linear carbonate,[9-12] nitrile, [8, 13-15] ester, [16-18] and ether[19, 20] functional groups. Recently, fluorination of solvents has drawn huge attention due to its improved oxidation stability and weak solvation features,[21-25] but is concerned about reduction instability and environmental pollution. These solvents in the electrolytes increase the ionic conductivity with lower activation energies, widening the operating temperatures of batteries. Among them, ester-based electrolytes have been reported to exhibit superior low-temperature performances due to the combined effect of the high ionic conductivity and low (de-)solvation energy.[6, 7]

Transference number (t_{Li^+}), defined by the contribution of conductivity of a specific charge carrier to the total ionic conductivity, plays a crucial role in the design of electrolytes. Conventional LIB electrolyte is composed of mixture solvents of a cyclic carbonate (EC) and

linear carbonate (DMC, DEC or EMC) dissolved in lithium salt ($LiPF_6$). In this solution, the high dielectric constant EC dissociates $LiPF_6$ into Li^+ and PF_6 anion, where Li^+ is tightly solvated with EC with molar ratio of 1 to 3 and 4. During the battery operation, the solvated Li^+-EC complex is bulkier and transported back and forth between the electrodes to support their redox reaction whereas the PF_6 anions are non-solvated and more mobile. The t_{Li}^+ is around 0.4, indicating PF_6 anion is the dominating ion carrier, not Li^+. To solve the fundamental issues of the fast charging and low temperature LIB, a new electrolyte with high t_{Li}^+ and high conductivity is required.[26, 27]

Since Li ions and anions are moving in opposite directions, the impact of t_{Li}^+ for the kinetics is normally interpreted in two ways. One is that the genuine Li ionic conductivity in the electrolytes can be calculated by multiplying the transference number and total ionic conductivity of the electrolyte. The other is that the anion-driven concentration overpotential can be observed at low Li transference number electrolytes. Since the mobile anions allow the diffusion-based conduction of each ion to electrodes, it leads to a Li depletion layer and high concentration overpotential, limiting the utilization of active materials across the electrodes.[28-31] To suppress the concentration overpotential, researchers have been devoted to developing electrolytes with high ionic conductivity and high t_{Li}^+, but it is challenging to enhance both properties due to their trade-off relationship. Although the near-unit t_{Li}^+ is observed in anion-anchored polymer electrolytes, they exhibit extremely low ionic conductivity due to the slow Li migration in the anion-anchored matrix.[32-37] In this regard, electrolytes with high ionic conductivity and transference number are pursued for high performance LIBs.

In this paper, we developed an anion-solvation dominated electrolyte with more mobile Li ions by using fluoride-transferred anion-based electrolytes to achieve the high Li^+ transference number electrolyte and demonstrated its superior properties in low-temperature LIBs. The fluoride transfer is induced by the chemical reaction of tris(pentafluorophenyl) borane (TPFPB) and LiF, in which the electron-deficient boron accepts the fluoride of LiF, dissociating the initially insoluble LiF salt. The fluoride transfer reaction was derived in various solvent systems, confirmed by mass spectroscopy. Both the high transference number of 0.848 and high ionic conductivity of 5.0 mS cm^{-1} were achieved in methyl acetate (MA) solvent electrolytes due to the bulky anions and solvent-dominant solvation structure. Molecular dynamics simulation revealed that the Li ions are weakly solvated by MA solvents and diffuse much faster than TPFPB-F complex anion, which in turn exhibit high transference numbers

and high ionic conductivity. This electrolyte, coupled with LiDFOB and FEC co-additive, yields a stable SEI passivation layer on the graphite anode surface and LIB using this optimized electrolyte displayed significantly improved cycling performances at a low temperature of −20 °C without any sign of Li plating. This result provides an insight on the potential of fluoride acceptors and fluoride-transferred anions for high transference number electrolytes and demonstrated the cell performance of insoluble LiF salt in lithium battery where graphite is used as anode for the first time.

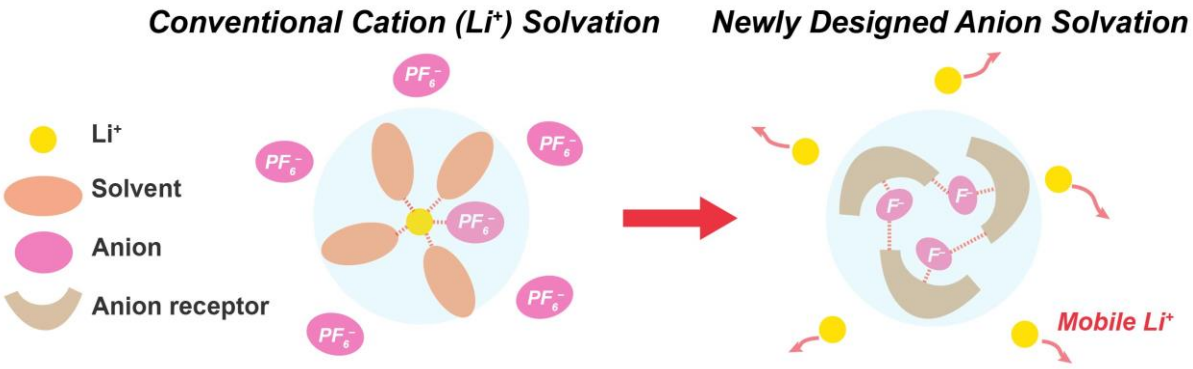

Scheme 1. Illustration of solvation structures of conventional electrolytes and newly designed electrolytes.

Scheme 1 illustrates a comparison between conventional cation (Li^+) solvation and a newly designed anion solvation approach. In the traditional cation solvation systems, Li ions are strongly bound by ethylene carbonate (EC) solvents and PF_6^- anions, leading to low transference numbers typically below 0.5. It is challenging to attain high transference numbers due to the bulky cation solvation structures and relatively rapid conduction of PF_6^- anions. In contrast, the newly designed anion solvation system is realized by incorporating anion receptors that accept fluoride ions (F^-), resulting in the formation of bulky anions and mobile Li ions. The solvent-dominant solvation structures have lower de-solvation energies and resultant lower anode overpotentials, suppressing Li plating at the graphite anodes. This innovative configuration aims to enhance Li^+ mobility and transference number by altering the solvation dynamics, improving ion transport and efficiency across a wide temperature range of LIBs.

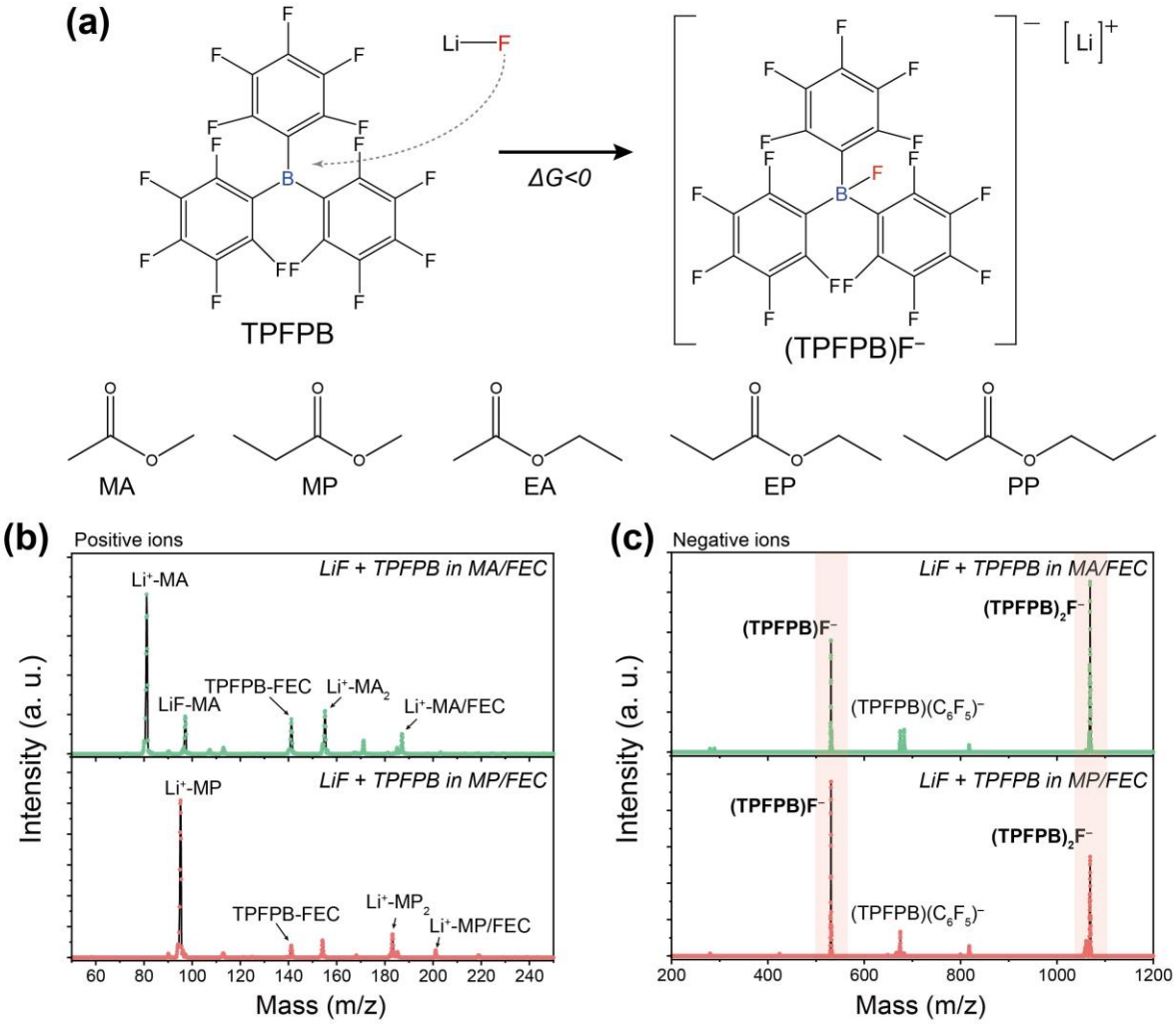

Figure 1. (a) Schematic illustration of fluoride transfer reaction between TPFPB and LiF. Mass spectroscopy in (b) positive ion and (c) negative ion mode of fluoride transfer reaction in MA or MP solvents.

Figure 1a illustrates the fluoride transfer induced by the reaction of tris(pentafluorophenyl) borane (TPFPB) and LiF. The boron center in TPFPB is electron-deficient and Lewis acidic and accepts the basic fluoride of LiF, generating a bulky anion of TPFPB-F^- complex.[38, 39] In addition, the fluoride-accepting power of TPFPB enables the disassociation and dissolution of LiF in electrolytes. The reaction was confirmed by density functional theory (DFT) calculation. The formation energy of the fluoride transfer was significantly negative (G=−2.12 eV), indicating that it is a thermodynamic reaction (**Figure S1a**). Among the fluoride acceptable positions, the boron center was revealed to be the most stable acceptor with the lowest formation energy (**Figure S1b**). The fluoride-transfer reaction of TPFPB and anion solvation

sheath were characterized by ESI-MS analysis (**Figures 1b and 1c**). Single solvent MA and MP were chosen to prepare the TPFPB-LiF electrolyte solution with 10% FEC added as SEI formation additive. Mixture of MA or MP with LiF powder was initially a suspension indicating insoluble LiF in these solvents, however the suspension became clear when TPFPB was added with agitation. 0.1 M TPFPB renders the LiF soluble, and 0.1M TPFPB + 0.3 M LiF in MA or MP was selected as the electrolyte for this study. The LiF and TPFPB concentrations were optimized to achieve both high ionic conductivity and transference number. In the MS spectra, the positive ions mode demonstrates that although there is a minor peak of LiF-MA, the Li ions are mostly solvated by MA or MP solvents, and TPFPB interacts with the fluorine in FEC from the presence of TPFPB-FEC peaks. The negative ions exhibit the strong peaks of fluoride transferred TPFPB, which are TPFPB-F^- and $(TPFPB)_2$-F^- in both cases. These theoretical and experimental results strongly support the fluoride-accepting reaction of TPFPB with LiF and the formation of TPFPB-F^- bulky anions.

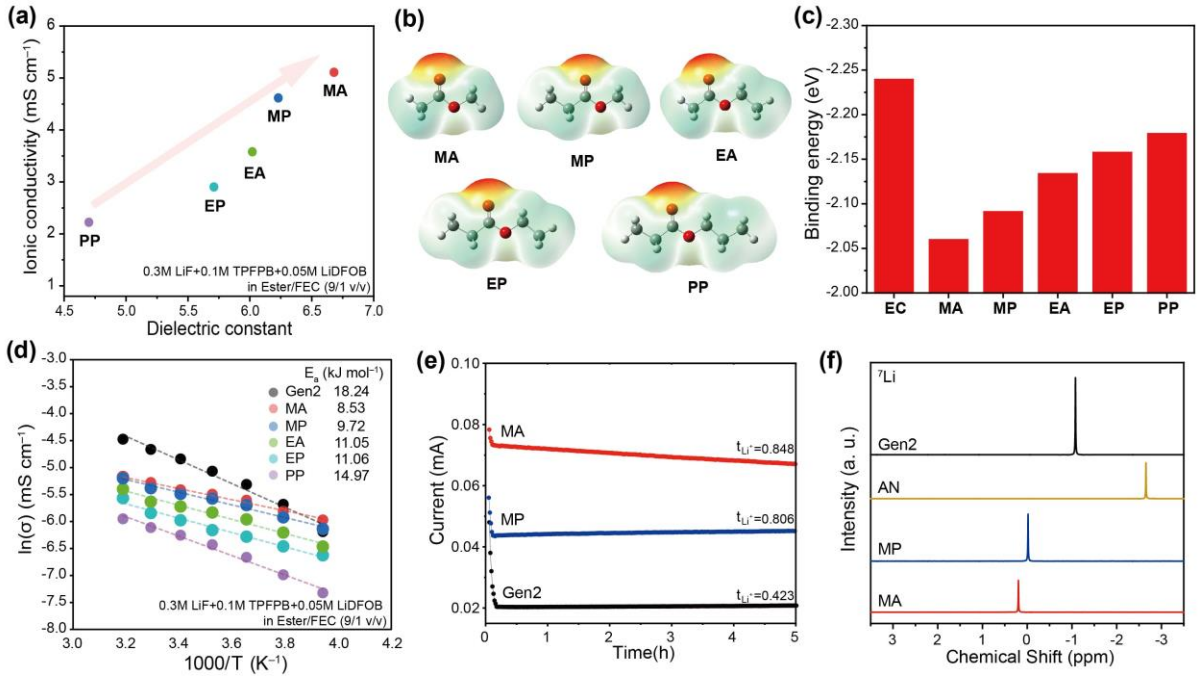

Figure 2. (a) Ionic conductivity of electrolytes with various ester solvents with respect to dielectric constant. (b) Electrostatic potential (ESP) surfaces of each solvent. (c) Binding energies of each solvent with a Li ion. (d) Activation energy for ionic conductivity of each electrolyte. (e) Transference number of Gen2 and fluoride-transferred electrolytes. (f) Chemical shift of 7Li in different electrolytes.

To enhance the physical properties of electrolytes such as ionic conductivity and t_{Li}^+, a variety

of ester solvents were screened based on the dielectric constant (**Figure 2a**). To note, 0.05 M LiDFOB was added as an additive owing to its low resistive SEI layer formation. The dielectric constants of ester solvents are linearly changed with alkyl chains from propyl propionate (PP) to methyl acetate (MA), and the ionic conductivities of electrolytes with those main solvents are correlated. As the dielectric constant of the solvent is higher, the ionic conductivity of the electrolyte is higher due to the solvent-dominant solvation of Li ions and low viscosity. To elucidate the binding configurations, electrostatic potential (ESP) surfaces of each solvent were generated (**Figure 2b**). All ester solvents exhibited high charge densities localized on the oxygen in the C=O group, indicating the preferential binding sites for interaction with Li ions. The binding energies for each solvent with a Li ion were calculated (**Figure 2c**). Among the solvents, MA demonstrated the weakest binding energy of −2.06 eV, which is considerably lower than that for EC solvent. The activation energy of each electrolyte was calculated by measuring the ionic conductivity at various temperatures (**Figure 2d**). There was a similar correlation between the dielectric constant of solvents and activation energy. Among the ester solvents, MA-based electrolytes showed the lowest activation energy of 8.53 kJ mol^{-1}, while PP-based electrolytes exhibited a much higher value of 14.97 kJ mol^{-1}. The low activation energy indicates the small change of ionic conductivity as temperature changes, enabling the electrolytes to be operable in a wide temperature range.

t_{Li}^+ plays a crucial role in determining the kinetics of electrolytes, especially at high current densities. The conventional anion-driven concentration overpotential with low t_{Li}^+ rapidly grows and limits the battery performance at low temperatures and high current densities.[8, 30] The t_{Li}^+ of MA, MP, and Gen2 electrolytes were measured by the Bruce-Vincent method (**Figures 2e and S2**).[40, 41] While Gen2 showed a low transference number of 0.423 due to the relatively fast diffusion of PF_6 anions, MA- and MP-based electrolytes exhibited much higher values of 0.848 and 0.806, respectively. Notably, the high t_{Li}^+ of the electrolytes is related to the immobilization of TPFPB-F^- likely due to the bulky size and its interaction with solvents. To study the Li-ion solvation structure of electrolytes, we conducted the nuclear magnetic resonance (NMR) characterization (**Figure 2f**). As a reference and baseline electrolyte for ^{7}Li-NMR measurement, Gen 2 and 1.0 M $LiClO_4$ in acetonitrile (AN) electrolytes were used, respectively. Since the Li ions are solvated by the solvent molecules and anions, the peak shift of ^{7}Li NMR represents the cumulative effect of the solvents and anion. The (downfield) positive shift of the ^{7}Li NMR spectra in the TPFPB-F^- systems compared with the baseline and reference electrolytes represents the weaker coordination of the Li-ion by the electronegative

solvents and less contribution of anions, suggesting a weak Li^+ solvation sheath. The strong down-field shift in the MA solvents suggests that the weak overall Li ion solvation is achieved in the MA electrolyte, which further promotes Li ion transportation kinetics.

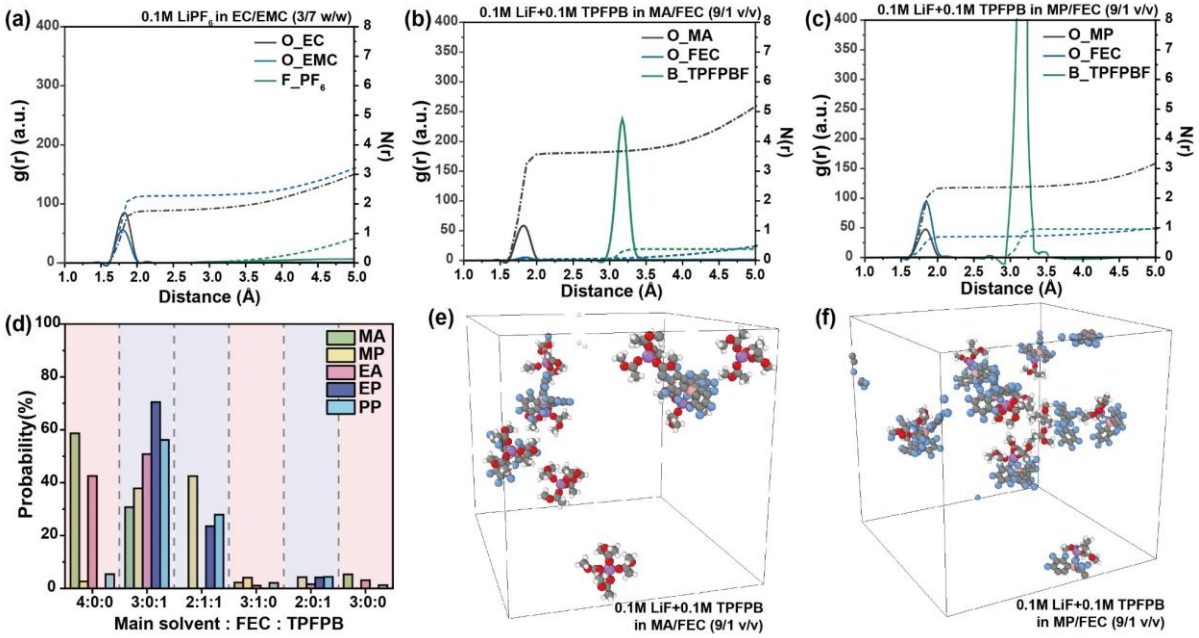

Figure 3. Radial distribution functions (RDF) of (a) Gen2_0.1 M, and fluoride-transferred Li salt in (b) MA or (c) MP solvents. (d) Probabilities of solvation structures in fluoride-transferred electrolytes with various ester solvents, in which solvent-separated ion pairs and contact ion pairs are colored in red and blue, respectively. Snapshots of Li solvation shells in fluoride-transferred Li salt in (e) MA or (f) MP solvent.

Classical molecular dynamics (MD) simulations were conducted to analyze the difference in ion diffusion coefficients at the atomic scale for electrolytes containing TPFPB-F ions (**Figure 3**). The LiF salt concentration in each electrolyte was set to 0.1 M to extract the effects of TPFPB-F ions and the primary solvents. RDF analysis was used to investigate the solvation structures around the Li ions (**Figures 3a-3c**). In the Gen2 (0.1 M $LiPF_6$) electrolyte, PF_6 anions exhibited minimal participation within the solvation structure (**Figure 3a**). However, in the 0.1 M TPFPB-F electrolyte, the anion coordination number was observed to be higher than that in the $LiPF_6$ electrolyte. It is evident that the complex TPFPB-F ions are formed by the fluoride-transfer reaction as shown in Figure 2. The TPFPB-F anions still exhibit a high localized charge density on the F atom even after the fluoride transfer reaction, leading to relatively strong binding between TPFPB-F anions and Li ions. Although the bulky size of the TPFPB-F anion

induces the steric hindrance to Li solvation, it competes with the binding of solvents in solvation structures.

The participation of TPFPF-F complex anions in the solvation structure varies with the primary ester solvents and their dielectric constants. For MA solvent, the anion coordination number showed the lowest value of 0.31 at 3.18 Å compared to other ester-based solvents, indicating minimal anion participation and relatively higher involvement of the MA solvent in the solvation structure (**Figure 3b**). In contrast, the anion coordination number in the MP solvent was nearly 1.0, with a value of 0.82 at the same position, indicating that most of the TPFPB-F ions were participating in the solvation structure (**Figure 3c**). The anion coordination numbers in EA, EP, and PP-based electrolytes were also higher than that of MA-based electrolytes (**Figure 3d**). The variations in contact ion pair (CIP) formation were influenced by the chain length of the solvents. MA solvent with short chain length and high dielectric constant exhibited the lowest probability of forming CIP structures, while other solvents with longer chains and low dielectric constant demonstrated an increased tendency for CIP formation due to the steric hinderance between solvents. This trend is also corresponding to the dielectric constant of solvents.

Using long-chain solvents such as MP, EP, and PP not only facilitates high anion coordination but also increases the coordination number of FEC in the Li ion solvation structure, with values of 0.59, 0.21, and 0.38, respectively (**Figures 3c and S3b-3c**). In most cases, FEC participates in the solvation structure with a composition of 2:1:1 (main solvent:FEC:anion) (**Figure S6**). This can be explained by the increase in steric hindrance induced by the anion in the CIP structure, which makes the relatively small FEC molecule likely to enter the first solvation shell. EA, on the other hand, exhibits a relatively low degree of CIP formation, and the coordination number of FEC is 0.02, indicating that FEC barely participates in the solvation structure (**Figure S3a**). To note, the TPFPB-F ions randomly interact with the main ester solvent and FEC. Although EA has the same chain length as MP and shows no significant difference in viscosity, it is known for EA to have a higher donor number.[42] RDF analysis also reveals that while other solvents exhibit a high peak with Li ions around 1.83 Å, EA shows a closer distance of approximately 1.80 Å, indicating stronger interactions with Li ions. This suggests that EA solvates Li ions more aggressively, reducing the CIP ratio and FEC's participation in the solvation structure. The solvation structures, visualized at a specific time point (**Figures 3e-3f**), demonstrate that MA-based electrolytes exhibit partial CIP formation

compared to other solvents.

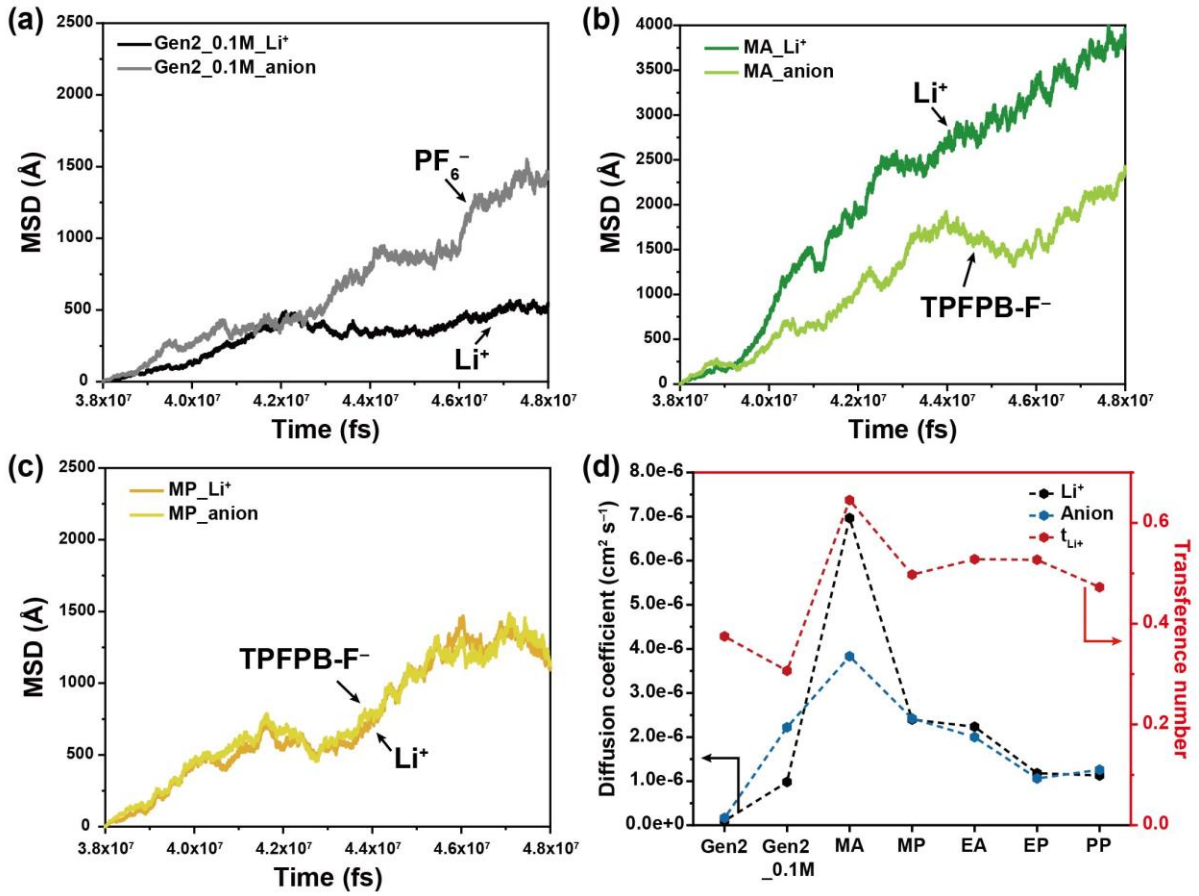

Figure 4. Mean squared displacement profiles of Li ions and anions in (a) Gen2, (b) MA-, and (c) MP-based electrolytes. (d) Diffusion coefficients and transference numbers of various electrolytes from MD simulations.

To compare the diffusion coefficients and transference numbers for each electrolyte, mean squared displacement (MSD) calculations were performed over 10 ns (**Figure 4**); details of the calculation parameters are provided in the Methods section. The diffusion coefficient of PF_6 anions is significantly larger than that of Li ions in Gen2 due to the large size of solvated Li ions (**Figure 4a**). However, in MA-based electrolytes, the Li ion diffusion coefficient was the highest at 6.97e-6 cm^2s^{-1}, and the transference number was also the highest at 0.65 (**Figure 4b**). In EP- and PP-based electrolytes, the CIP moves together, as evidenced by similar MSD behavior of Li ions and TPFPB-F ions (**Figures S4-S5**). Consequently, the transference numbers for EP and PP solvents were 0.53 and 0.47, respectively, approaching 0.50. While MP

solvents exhibited lower viscosity compared to EP and PP and higher diffusion coefficients for both cations and anions, the high CIP ratio in MP electrolytes results in a transference number of 0.50 (**Figure 4c**). In EA-based electrolytes, although the SSIP ratio is higher than those of other longer-chain solvents, the strong interactions between the solvent and Li ions lead to lower diffusivity compared to MA and MP. In MA-based solvents, partial CIP formation and the high participation of primary solvents in the solvation structure led to distinct behaviors of ions and high transference number (**Figure 4d**). These characteristics significantly enhance Li-ion diffusion and increase the transference number.

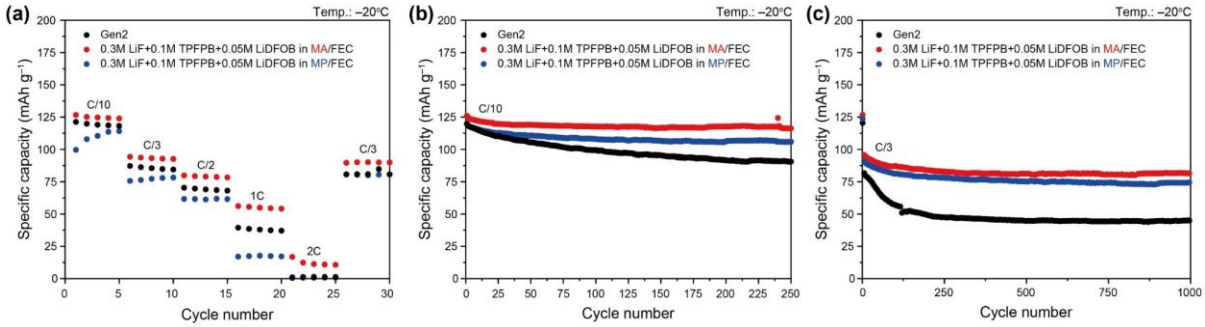

Figure 5. (a) C-rate capabilities of Gen2, MA and MP electrolytes at temperature of −20°C. Cycling performances of Gen2, MA and MP electrolytes at C-rates of (b) C/10 or (c) C/3 at a temperature of −20°C.

The peculiar conduction behavior of MA/LiF/TPFPB electrolyts was reflected in their lithium-ion battery performance (**Figure 5**). In the differential capacity dQ/dV profiles of the TPFPB-F electrolytes, the peak of LiDFOB additive reduction was observed at 2.25 V (**Figure S7**), indicating the electrochemical stability of TPFPB and the formation of stable DFOB-driven SEI layers on the graphite anodes. This also indicates that the electrochemical performances between the TPFPB-F electrolytes are determined by the conduction behaviors. To note, the amount of LiF was suppressed by the fluoride-accepting power of TPFPB in the XPS analysis (**Figure S8**). The rate capability of Gen2, MA, and MP electrolytes was measured at a low temperature of −20°C. The MA electrolyte showed the highest discharge capacity of 56.1 mAh/g at 1 C rate, while Gen2 and MP electrolytes exhibited limited capacities of 39.4 mAh/g and 17.0 mAh/g, respectively. This is due to the combined effect of high transference number and ionic conductivity of MA electrolyte. When comparing the cells with Gen2 and MP

electrolyte, the overpotential of Gen2 was slightly lower than that of MP electrolyte, resulting in a better rate capability (**Figure S9**). The superior performance was also confirmed by long-term cyclability at low temperature of −20ºC (**Figures 5b-5c**). The MA electrolyte showed an exceptionally stable cycling performance with a high-capacity retention of 92.2% after 250 cycles, indicating a limited lithium plating due to the low overpotentials at low temperatures (**Figure S10**). The high stability of MA electrolyte was continued at an elevated rate of C/3, exhibiting an extremely high capacity retention of 85.1% even after 1000 cycles. The superior performance of the MA electrolyte was also confirmed by rate capability at a lower temperature of −40ºC (**Figure S11**).

In conclusion, we have developed a novel electrolyte system based on the fluoride-acceptor tris(pentafluorophenyl) borane (TPFPB) and LiF salt in ester-based solvents. The fluoride transfer reaction, driven by the electron-deficient boron center in TPFPB, enabled the dissociation of otherwise insoluble LiF, as confirmed by mass spectrometry and NMR analysis. The resulting fluoride-transferred anions (TPFPB-F^-) introduced unique ion transport mechanisms, enhancing both the lithium-ion transference number and ionic conductivity. Notably, an exceptionally high transference number of 0.848 and ionic conductivity of 5.0 mS cm^{-1} were achieved in methyl acetate (MA)-based electrolytes, attributed to MA's high dielectric constant and solvent-dominated solvation structure—properties difficult to attain in conventional liquid electrolytes. Molecular dynamics simulations further revealed that Li^+ ions are strongly solvated by MA, resulting in significantly higher diffusion coefficients compared to TPFPB-F^- anions. The optimized electrolyte, incorporating LiDFOB as an additive and FEC as a co-solvent, formed a stable solid electrolyte interphase (SEI) on graphite anodes and delivered superior performance at −20 °C without any indication of lithium plating. This work provides new insight into the role of fluoride-transferred anions in achieving high transference number electrolytes, advancing the development of low-temperature, fast-charging lithium-ion batteries and beyond.

Methods

X-ray photoelectron spectroscopy (XPS):

XPS analysis was conducted on a PHI 5000 VersaProbe II system (Physical Electronics) with a base pressure of ~2×10^{-9} torr. The spectra were obtained using an Al Kα radiation (hυ=1486.6 eV) beam (100 μm, 25 W), with Ar^+ and electron beam sample neutralization, in Fixed Analyzer Transmission mode with a pass energy of 11.75 eV. Subtracting a Shirley background and then fitting the spectra to multiple Gaussian peaks was performed on all spectra using the Multipack software from Physical Electronics. The area under the XPS peaks (the sum of the Gaussian components) was adjusted using manufacturer-calibrated relative sensitivity factors and normalized to obtain elemental concentrations. The same normalization factors were used to plot XPS signal intensities as concentration per unit energy (at % eV^{-1}). Binding energy was calibrated by shifting every region to align the C 1s peak of C-C/C-H environments at 284.8 eV.

Computational Simulation:

Molecular dynamics (MD) simulations were conducted using LAMMPS to analyze the diffusivity and solvation structures of various electrolytes. The OPLS-AA force field[43] was applied to all molecules, and coulombic interactions were obtained using CHELPG[44] charges calculated at the MP2/aug-cc-pVTZ level of theory with Gaussian 16 software. Missing intermolecular parameters, such as those for boron, were obtained from references[45, 46] and validated through relaxed potential energy surface scans. The force field parameters for Li^+ and $PF6^-$ were derived from references.[47] The systems were constructed using Packmol[48] to randomly distribute molecules according to their volume ratios, weight ratios, and molar concentrations: (1) EC/EMC 3/7 (w/w) 1.2M LiPF6 : 259/512/96, (2) EC/EMC 3/7 (w/w) 0.1M $LiPF_6$: 292/577/8, (3) MA/FEC (9/1 v/v) 0.1M Li(TPFPB-F) : 843/104/8, (4) MP/FEC (9/1 v/v) 0.1M Li(TPFPB-F) : 695/104/8, (5) EA/FEC (9/1 v/v) 0.1M Li(TPFPB-F) : 685/104/8, (6) EP/FEC (9/1 v/v) 0.1M Li(TPFPB-F) : 582/104/8, (7) PP/FEC (9/1 v/v) 0.1M Li(TPFPB-F) : 507/104/8. Periodic boundary conditions were applied to represent bulk electrolyte environments, and a time step of 1 fs was used. A cutoff distance of 1.2 nm was applied for Lennard-Jones interactions, while long-range interactions were calculated using the particle-particle-particle mesh (PPPM) method. Initial equilibration was performed for 2 ns under the NPT ensemble at 298.15 K and 1 atm. A thermal treatment process followed, where the

temperature gradually increased to 500.15 K over 1 ns and maintained for another 1 ns under the NVT ensemble, before being slowly reduced back to 298.15 K. The system was further equilibrated for 33 ns under the NVT ensemble at 298.15 K to achieve thermal equilibrium. After a total equilibration period of 38 ns, diffusivity and solvation structures were analyzed for over a 10 ns interval from 38 ns to 48 ns. Solvation structure probabilities were calculated from trajectory files over a 5 ns interval (43 ns to 48 ns) at 0.01 ns intervals to derive average probabilities. Snapshots of solvation structures for each electrolyte were visualized at 48 ns. Diffusion coefficients were calculated using the following equation:

$$D_{ion} = \lim_{t\to\infty} \frac{MSD(t)}{6t},\ t_{Li^+} = \frac{D_{Li^+}}{D_{Li^+} + D_{PF_6^-\ or\ TPFPB-F^-}}$$

Acknowledgements

This work was funded by the U.S. Department of Energy (DOE), Office of Energy Efficiency and Renewable Energy, Vehicle Technologies Office. This research used the Leadership Computing Facility resource at Argonne National Laboratory, which is supported by DOE Office of Science under Contract No. DE-AC02-06CH11357. D.-J.Y. acknowledges technical support from the Supercomputing Center/Korea Institute of Science and Technology Information (KSC-2024-CRE-0068).

Author contributions

Z.Z. conceived the project. M.A.H., D.W., Z.Y., and S.-B.S. carried out the experiments. J.X., C.L., S.K. and D.-J.Y. designed and conducted the simulations. Q.Z., J.Y. and Q.L. analyzed the experimental data. The manuscript was written with contributions from all authors.

Supporting Information

Material preparation; electrochemical measurement and characterization; binding energy of F^- and TPFPB; EIS spectra; MD simulation data; XPS spectra; cell performance at -40 ^oC and post-test analysis

References

1. Choi, J. W.; Aurbach, D., Promise and reality of post-lithium-ion batteries with high energy densities. *Nature Reviews Materials* **2016,** *1* (4), 16013.
2. Hou, R.; Guo, S.; Zhou, H., Atomic Insights into Advances and Issues in Low-Temperature Electrolytes. *Advanced Energy Materials* **2023,** *13* (14), 2300053.
3. Huh, S.-H.; Yang, S. J.; Nam, J.; Shin, M.; Yoo, D.-J.; Yu, S.-H., Current trends and recent strategies to overcome battery safety issues. *Journal of Industrial and Engineering Chemistry* **2025**, 149, 157-175.
4. Chen, L.; Wu, H.; Ai, X.; Cao, Y.; Chen, Z., Toward wide-temperature electrolyte for lithium–ion batteries. *Battery Energy* **2022,** *1* (2), 20210006.
5. Hubble, D.; Brown, D. E.; Zhao, Y.; Fang, C.; Lau, J.; McCloskey, B. D.; Liu, G., Liquid electrolyte development for low-temperature lithium-ion batteries. *Energy & Environmental Science* **2022,** *15* (2), 550-578.
6. Li, Z.; Yao, Y.-X.; Sun, S.; Jin, C.-B.; Yao, N.; Yan, C.; Zhang, Q., 40 Years of Low-Temperature Electrolytes for Rechargeable Lithium Batteries. *Angewandte Chemie International Edition* **2023,** *62* (37), e202303888.
7. Su, X.; Xu, Y.; Wu, Y.; Li, H.; Yang, J.; Liao, Y.; Qu, R.; Zhang, Z., Liquid electrolytes for low-temperature lithium batteries: main limitations, current advances, and future perspectives. *Energy Storage Materials* **2023,** *56*, 642-663.
8. Yoo, D.-J.; Liu, Q.; Cohen, O.; Kim, M.; Persson, K. A.; Zhang, Z., Understanding the Role of SEI Layer in Low-Temperature Performance of Lithium-Ion Batteries. *ACS Applied Materials & Interfaces* **2022,** *14* (9), 11910-11918.
9. Smart, M. C.; Ratnakumar, B. V.; Whitcanack, L. D.; Chin, K. B.; Surampudi, S.; Croft, H.; Tice, D.; Staniewicz, R., Improved low-temperature performance of lithium-ion cells with quaternary carbonate-based electrolytes. *Journal of Power Sources* **2003,** *119-121*, 349-358.
10. Chen, Y.; He, Q.; Zhao, Y.; Zhou, W.; Xiao, P.; Gao, P.; Tavajohi, N.; Tu, J.; Li, B.; He, X.; Xing, L.; Fan, X.; Liu, J., Breaking solvation dominance of ethylene carbonate via molecular charge engineering enables lower temperature battery. *Nature Communications* **2023,** *14* (1), 8326.
11. Kondou, S.; Sakashita, Y.; Yang, X.; Hashimoto, K.; Dokko, K.; Watanabe, M.; Ueno, K., Li-Ion Transport and Solvation of a Li Salt of Weakly Coordinating Polyanions in Ethylene Carbonate/Dimethyl Carbonate Mixtures. *ACS Applied Materials & Interfaces* **2022,** *14* (16), 18324-18334.
12. Zhang, S. S.; Xu, K.; Allen, J. L.; Jow, T. R., Effect of propylene carbonate on the low temperature performance of Li-ion cells. *Journal of Power Sources* **2002,** *110* (1), 216-221.
13. Langevin, S. A.; McGuire, M. M.; Le, N. Q.; Ragasa, E.; Hamann, T.; Ferguson, G.; Chung, C.; Domenico, J.; Ko, J. S., Developing a nitrile-based lithium-conducting electrolyte for low temperature operation. *Journal of Materials Chemistry A* **2022,** *10* (37), 19972-19983.
14. Luo, L.; Chen, K.; Chen, H.; Li, H.; Cao, R.; Feng, X.; Chen, W.; Fang, Y.; Cao, Y., Enabling Ultralow-Temperature (−70 °C) Lithium-Ion Batteries: Advanced Electrolytes Utilizing Weak-Solvation and Low-Viscosity Nitrile Cosolvent. *Advanced Materials* **2024,** *36* (5), 2308881.
15. Wang, Z.; He, Z.; Wang, Z.; Yang, J.; Long, K.; Wu, Z.; Zhou, G.; Mei, L.; Chen, L., A nitrile solvent structure induced stable solid electrolyte interphase for wide-temperature lithium-ion batteries. *Chemical Science* **2024,** *15* (34), 13768-13778.
16. Cho, Y.-G.; Li, M.; Holoubek, J.; Li, W.; Yin, Y.; Meng, Y. S.; Chen, Z., Enabling the Low-Temperature Cycling of NMC||Graphite Pouch Cells with an Ester-Based Electrolyte. *ACS Energy Letters* **2021,** *6* (5), 2016-2023.
17. Lai, P.; Huang, B.; Deng, X.; Li, J.; Hua, H.; Zhang, P.; Zhao, J., A localized high concentration carboxylic ester-based electrolyte for high-voltage and low temperature lithium batteries. *Chemical Engineering Journal* **2023,** *461*, 141904.
18. Yang, S. J.; Kang, S.; Koo, J.-H.; Lee, G.-J.; Lim, S.-G.; Kim, J.-S.; Jin, K.; Kim, H. W.; Yoon, H.; Yoo, D.-J., Development of non-fluorinated hybrid ester solvents for wide-temperature operation of lithium-ion batteries. *Journal of Materials Chemistry A* **2025,** *13* (11), 7692-7699.
19. Li, Z.; Liu, J.; Bi, X.; Qin, Y.; Gao, T., Single-oxygen linear ether (SOLE) based electrolytes for fast-charging and low-temperature Li-ion batteries. *Journal of Materials Chemistry A* **2023,** *11* (37), 19996-20010.
20. Wang, S.; Shi, J.; Liu, Z.; Xia, Y., Advanced Ether-Based Electrolytes for Lithium-ion Batteries. *Advanced Energy Materials* **2024,** *14* (37), 2401526.
21. Holoubek, J.; Yu, M.; Yu, S.; Li, M.; Wu, Z.; Xia, D.; Bhaladhare, P.; Gonzalez, M. S.; Pascal, T. A.; Liu, P.; Chen, Z., An All-Fluorinated Ester Electrolyte for Stable High-Voltage Li Metal Batteries Capable of Ultra-Low-Temperature Operation. *ACS Energy Letters* **2020,** *5* (5), 1438-1447.
22. Mo, Y.; Liu, G.; Yin, Y.; Tao, M.; Chen, J.; Peng, Y.; Wang, Y.; Yang, Y.; Wang, C.; Dong, X.; Xia,

Y., Fluorinated Solvent Molecule Tuning Enables Fast-Charging and Low-Temperature Lithium-Ion Batteries. *Advanced Energy Materials* **2023,** *13* (32), 2301285.
23. Yoo, D.-J.; Liu, Q.; Cohen, O.; Kim, M.; Persson, K. A.; Zhang, Z., Rational Design of Fluorinated Electrolytes for Low Temperature Lithium-Ion Batteries. *Advanced Energy Materials* **2023,** *13* (20), 2204182.
24. Zhang, G.; Chang, J.; Wang, L.; Li, J.; Wang, C.; Wang, R.; Shi, G.; Yu, K.; Huang, W.; Zheng, H.; Wu, T.; Deng, Y.; Lu, J., A monofluoride ether-based electrolyte solution for fast-charging and low-temperature non-aqueous lithium metal batteries. *Nature Communications* **2023,** *14* (1), 1081.
25. Fan, X.; Ji, X.; Chen, L.; Chen, J.; Deng, T.; Han, F.; Yue, J.; Piao, N.; Wang, R.; Zhou, X.; Xiao, X.; Chen, L.; Wang, C., All-temperature batteries enabled by fluorinated electrolytes with non-polar solvents. *Nature Energy* **2019,** *4* (10), 882-890.
26. Cai, W.; Yao, Y.-X.; Zhu, G.-L.; Yan, C.; Jiang, L.-L.; He, C.; Huang, J.-Q.; Zhang, Q., A review on energy chemistry of fast-charging anodes. *Chemical Society Reviews* **2020,** *49* (12), 3806-3833.
27. Xu, K., Electrolytes and Interphases in Li-Ion Batteries and Beyond. *Chemical Reviews* **2014,** *114* (23), 11503-11618.
28. Bai, P.; Li, J.; Brushett, F. R.; Bazant, M. Z., Transition of lithium growth mechanisms in liquid electrolytes. *Energy & Environmental Science* **2016,** *9* (10), 3221-3229.
29. Jana, A.; Woo, S. I.; Vikrant, K. S. N.; García, R. E., Electrochemomechanics of lithium dendrite growth. *Energy & Environmental Science* **2019,** *12* (12), 3595-3607.
30. Thomas, K. E.; Sloop, S. E.; Kerr, J. B.; Newman, J., Comparison of lithium-polymer cell performance with unity and nonunity transference numbers. *Journal of Power Sources* **2000,** *89* (2), 132-138.
31. Xu, X.; Liu, Y.; Hwang, J.-Y.; Kapitanova, O. O.; Song, Z.; Sun, Y.-K.; Matic, A.; Xiong, S., Role of Li-Ion Depletion on Electrode Surface: Underlying Mechanism for Electrodeposition Behavior of Lithium Metal Anode. *Advanced Energy Materials* **2020,** *10* (44), 2002390.
32. Huo, H.; Wu, B.; Zhang, T.; Zheng, X.; Ge, L.; Xu, T.; Guo, X.; Sun, X., Anion-immobilized polymer electrolyte achieved by cationic metal-organic framework filler for dendrite-free solid-state batteries. *Energy Storage Materials* **2019,** *18*, 59-67.
33. Shao, Y.; Gudla, H.; Mindemark, J.; Brandell, D.; Zhang, C., Ion Transport in Polymer Electrolytes: Building New Bridges between Experiment and Molecular Simulation. *Accounts of Chemical Research* **2024,** *57* (8), 1123-1134.
34. Snyder, R. L.; Choo, Y.; Gao, K. W.; Halat, D. M.; Abel, B. A.; Sundararaman, S.; Prendergast, D.; Reimer, J. A.; Balsara, N. P.; Coates, G. W., Improved Li+ Transport in Polyacetal Electrolytes: Conductivity and Current Fraction in a Series of Polymers. *ACS Energy Letters* **2021,** *6* (5), 1886-1891.
35. Wang, Y.; Fu, L.; Shi, L.; Wang, Z.; Zhu, J.; Zhao, Y.; Yuan, S., Gel Polymer Electrolyte with High Li+ Transference Number Enhancing the Cycling Stability of Lithium Anodes. *ACS Applied Materials & Interfaces* **2019,** *11* (5), 5168-5175.
36. Zhang, T.; Zhang, J.; Yang, S.; Li, Y.; Dong, R.; Yuan, J.; Liu, Y.; Wu, Z.; Song, Y.; Zhong, Y.; Xiang, W.; Chen, Y.; Zhong, B.; Guo, X., Facile In Situ Chemical Cross-Linking Gel Polymer Electrolyte, which Confines the Shuttle Effect with High Ionic Conductivity and Li-Ion Transference Number for Quasi-Solid-State Lithium–Sulfur Battery. *ACS Applied Materials & Interfaces* **2021,** *13* (37), 44497-44508.
37. Zhao, Y.; Wang, L.; Zhou, Y.; Liang, Z.; Tavajohi, N.; Li, B.; Li, T., Solid Polymer Electrolytes with High Conductivity and Transference Number of Li Ions for Li-Based Rechargeable Batteries. *Advanced Science* **2021,** *8* (7), 2003675.
38. Erker, G., Tris(pentafluorophenyl)borane: a special boron Lewis acid for special reactions. *Dalton Transactions* **2005,** (11), 1883-1890.
39. Li, L. F.; Lee, H. S.; Li, H.; Yang, X. Q.; Nam, K. W.; Yoon, W. S.; McBreen, J.; Huang, X. J., New electrolytes for lithium ion batteries using LiF salt and boron based anion receptors. *Journal of Power Sources* **2008,** *184* (2), 517-521.
40. Bruce, P. G.; Evans, J.; Vincent, C. A., Conductivity and transference number measurements on polymer electrolytes. *Solid State Ionics* **1988,** *28-30*, 918-922.
41. Bruce, P. G.; Hardgrave, M. T.; Vincent, C. A., The determination of transference numbers in solid polymer electrolytes using the Hittorf method. *Solid State Ionics* **1992,** *53-56*, 1087-1094.
42. Qin, Y.; Choi, S.-G.; Mason, L.; Liu, J.; Li, Z.; Gao, T., Carboxylate ester-based electrolytes for Na-ion batteries. *Chemical Science* **2024,** *15* (24), 9224-9239.
43. Jorgensen, W. L.; Maxwell, D. S.; Tirado-Rives, J., Development and Testing of the OPLS All-Atom Force Field on Conformational Energetics and Properties of Organic Liquids. *Journal of the American Chemical Society* **1996,** *118* (45), 11225-11236.
44. Breneman, C. M.; Wiberg, K. B., Determining atom-centered monopoles from molecular electrostatic potentials. The need for high sampling density in formamide conformational analysis. *Journal of Computational Chemistry* **1990,** *11* (3), 361-373.

45. Doherty, B.; Zhong, X.; Gathiaka, S.; Li, B.; Acevedo, O., Revisiting OPLS Force Field Parameters for Ionic Liquid Simulations. *Journal of Chemical Theory and Computation* **2017,** *13* (12), 6131-6145.
46. Shurvell, H. F.; Faniran, J. A., Infrared spectra of triphenylboron and triphenylborate. *Canadian Journal of Chemistry* **1968,** *46* (12), 2081-2087.
47. Dang, L. X., Development of nonadditive intermolecular potentials using molecular dynamics: Solvation of Li+ and F− ions in polarizable water. *The Journal of Chemical Physics* **1992,** *96* (9), 6970-6977.
48. Martínez, L.; Andrade, R.; Birgin, E. G.; Martínez, J. M., PACKMOL: A package for building initial configurations for molecular dynamics simulations. *Journal of Computational Chemistry* **2009,** *30* (13), 2157-2164.